NJC

Accepted Manuscript

This is an *Accepted Manuscript*, which has been through the Royal Society of Chemistry peer review process and has been accepted for publication.

Accepted Manuscripts are published online shortly after acceptance, before technical editing, formatting and proof reading. Using this free service, authors can make their results available to the community, in citable form, before we publish the edited article. We will replace this *Accepted Manuscript* with the edited and formatted *Advance Article* as soon as it is available.

You can find more information about *Accepted Manuscripts* in the Information for Authors.

Please note that technical editing may introduce minor changes to the text and/or graphics, which may alter content. The journal's standard Terms & Conditions and the Ethical guidelines still apply. In no event shall the Royal Society of Chemistry be held responsible for any errors or omissions in this *Accepted Manuscript* or any consequences arising from the use of any information it contains.

ROYAL SOCIETY OF CHEMISTRY

www.rsc.org/njc

NJC

RSCPublishing

PAPER

Molecular structure, spectral analysis and hydrogen bonding analysis of ampicillin trihydrate: A combined DFT and AIM approach

Cite this: DOI: 10.1039/c3nj00000x

Eram Khan,[a] Anuradha Shukla,[a] Anubha Srivastava,[a] Shweta[a] and Poonam Tandon*[a]

Received 00th XXXXX 2013,
Accepted 00th XXXXX 2013

DOI: 10.1039/c3nj00000x

Ampicillin trihydrate chemically associated to $C_{16}H_{19}N_3O_4S{\cdot}3H_2O$ empirical formula, is a semi-synthetic amino-penicillin derived from the elementary penicillin nucleus, 6-aminopenicillanic acid. It is a very common antibiotic that is active against an extensive range of Gram-positive and Gram-negative organisms. It is used to treat certain varieties of bacterial infections, like gonorrhea and infections of the urinary, intestinal and respiratory tracts. In the present effort, quantum chemical calculations of molecular geometries (bond lengths and bond angles) and bonding features of monomer and dimer of ampicillin trihydrate in the ground state have been carried out due to its biological and industrial importance. The optimized geometry and wavenumber of the vibrational bands of the molecule have been calculated by *ab-initio* density functional theory (DFT) using Becke's three-parameters hybrid functional (B3LYP) with 6–311++G(d,p) basis set. Vibrational wavenumbers were compared with the observed FT-Raman and FT-IR spectra. Molecular electrostatic potential (MEP) has also been plotted for predicting the molecule reactivity towards positively or negatively charged reactants and it shows that electropositive potential is visualized in the vicinity of the $-NH_3$ group and electropositive region is found near the H_2O molecule in both monomer and dimer. HOMO-LUMO analysis has been done to describe the way the molecule interacts with other species. Natural bond orbitals (NBO) analysis has been carried out to inspect the intra- and inter- molecular hydrogen-bonding, conjugative and hyperconjugative interactions and their second order stabilization energy $E^{(2)}$. Nonlinear optical (NLO) analysis has also been performed to study the non-linear optical properties of the molecule by computing the first hyperpolarizability (β_0). The variation of thermodynamic properties with temperature has been studied. Topological parameters at bond critical points (BCP) have been evaluated by 'Quantum theory of atoms in molecules' (QTAIM).

www.rsc.org/njc

1. Introduction

Antibiotics are definite chemical substances which are resultant of or produced by living organisms like bacteria and fungi that are skilled with killing, or preventing the life processes of other organisms[1,2]. One such group of antibiotics is penicillins that are consumed to treat a wide range of bacterial infections occurring within the body[1]. A kind of fungi called Penicillium fungi produces them. These antibiotics are renowned in medicine as they are one of the first kinds of antibiotic used for main infections and diseases, and are still used commonly in present medicine. All of the penicillins are β-lactam antibiotics and are effectively used in the cure of bacterial infections caused by susceptible, usually Gram-positive, organisms[3]. The aminopenicillins, which is a group of antibiotics[4], in the penicillin family, have a β-lactam ring, and prevent the synthesis of bacterial cell walls. They are the first penicillins found to be active against Gram-negative bacteria. Changes in the structure of penicillins were done so as to increase the spectrum of the penicillins in order to include inhibition of Gram-negative bacteria derivatives. The first and foremost development in this approach was ampicillin, which offered a broader spectrum of activity than any of the original penicillins. Ampicillin crystals, according to the level of hydration, usually exist in four forms, anhydrate (form I and form II), monohydrate and trihydrate[5-8]. This medicine is on the World Health Organization's List of Essential Medicines[9].

The title compound, ampicillin trihydrate (AT) chosen for this study is a significant heterocyclic compound which is strongly hydrogen bonded in the solid state. AT is formed when crystallization of ampicillin from aqueous solution at temperatures below 50℃ is done , while crystallization from aqueous solution at

temperatures above 60℃ yields the anhydrate form[10,11]. An intact β-lactam/thiazolidine fused ring system was supposed to be important for antibiotic action. AT, consists of a thiazolidine ring attached to a β-lactam ring and a unique side chain that distinguishes it from the other antibiotics[12]. It has been used as broad-spectrum semi-synthetic penicillin which is effective in the cure of Gram-positive and Gram-negative bacterial infections produced by Haemophilus influenza, Streptococcus, Neisseria gonorrhoeae, Bacillus anthracis, and Escherichia coli[13]. It is also considered for treatment of urinary tract infections (UTI) caused by susceptible enterococci, E. coli, or Proteus mirabilis[9,14]. It is used as a substitute for the cure of typhoid fever (enteric fever) caused by susceptible Salmonella typhi[14].

Ampicillin trihydrate is labelled chemically as (2S, 5R, 6R)-6-[(R)-2-Amino-2-phenylacetamido]-3, 3-dimethyl-7-oxo-4-thia-l-azabicyclo [3.2.0] heptane-2-carboxylic acid trihydrate. The chemical structure of AT is shown in Fig. 1. It occurs essentially as white, odourless, crystalline powder that is feebly soluble in water. AT is the most stable form in water at room temperature[15]. In the trihydrate form the amino group is hydrogen bonded to a single carboxyl group with a complicated arrangement of the three hydrogen-bonded water molecules which also form hydrogen bonds to three further atoms within the molecule. AT belongs to an orthorhombic system, space group $P2_12_12_1$ with cell parameters a = 15.52275 (16) Å, b = 18.9256 (3) Å, c = 6.67375 (8) Å, z = 4[16]. The molecule is zwitterions.

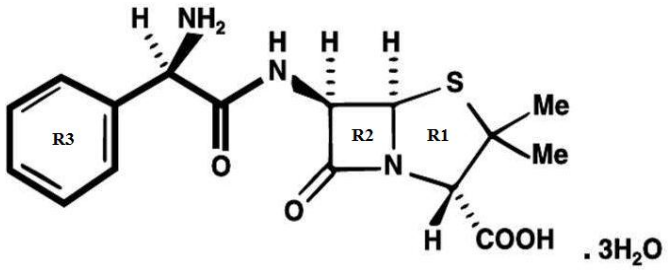

Fig. 1 Chemical structure of AT.

Vibrational spectroscopic (infrared[17] and Raman[18]) methods are particularly essential for the characterization of supramolecular complexes. Thus in the present study, the FT-IR and FT-Raman spectra of AT have analysed by matching them with the ones calculated using *ab-initio* density functional theory (DFT). Baraldi et al.[19] have recently reported vibrational study of monomer of AT based on DFT calculations. However, they have not given the complete potential energy distribution (PED) of the vibrational modes and the comparison between calculated and observed wavenumbers of the spectra of the AT. In addition, they have not considered the intermolecular hydrogen bonding that plays a significant role to stabilize the molecular structure. Vibrational spectroscopy and quantum theory of atoms in molecules (QTAIM) calculations are few approaches that directly conclude on the strength of hydrogen bonds. In the present work, the effects of hydrogen bonding on the Raman and IR spectrum of AT have been examined by DFT calculations on monomer as well as hydrogen bonded dimer. Crystal structure of AT[16] has been used to construct the hydrogen bonded model dimer. The aim of this study is to fully determine the optimized geometries, atomic charges and vibrational spectra for the AT molecule and examine the different normal modes of the AT molecule. The vibrational frequencies of AT are allocated to their corresponding normal vibration mode by means of PEDs.

In order to give clear evidence of stabilization originating from the hyperconjugation of various intra- and inter- molecular interactions, the redistribution of electron density (ED) in various bonding, antibonding orbitals and $E^{(2)}$ energies has been computed by natural bond orbital (NBO) analysis. The HOMO, LUMO study has been used to expose the information concerning charge transfer within the molecule. The molecular electrostatic potential surface (MEP) of the compound is useful for understanding the connection between biological activity and molecular structure. DFT and QTAIM methods have been applied to gain a deeper understanding into the nature of intra- and inter- molecular interactions. This analysis allowed us to estimate the strength of the hydrogen bonding.

2. Experimental details

2.1. Fourier transform-infrared spectroscopy

The spectrum was recorded with the help of a VERTEX 70 (Bruker) FT-IR spectrophotometer with a spectral resolution of 4 cm^{-1} in the region 600–4000 cm^{-1} to get qualitative information about the functional groups present in a sample. FT-IR spectrophotometer was fitted with a mercury-cadmium-telluride (MCT) detector. Setting parameter: apodization function is [cos(t); 1 − (t/T); 1 − (t −T)2]. The spectrum was accumulated for 32 scans. Multi-tasking OPUS software was used for base line corrections.

2.2. Fourier transform-Raman spectroscopy

FT-Raman spectrum was recorded by using a Bruker multiram spectrometer, equipped with a FRA 106 FT-Raman module and with a near IR continuous-wave Nd-YAG laser operating at 1064 nm in backscattering. The laser was focused on the sample as an approximately 100 μm x 100 μm area and a liquid nitrogen-cooled germanium detector was used. The FT-Raman spectrum of this compound was recorded in the region 100–3500 cm^{-1}. Typical spectrum was acquired with nearly 2000 scans with a resolution of 4 cm^{-1} was averaged for the sample.

3. Computational Details

Theoretical methods and basis sets have to be incorporated in order to meet up the requirements of both precision and computing budget. For this DFT has proved to be particularly advantageous in treating electronic structure of molecules.

The complete vibrational spectra, molecular geometry optimizations and molecular electrostatic potential calculations of monomer and dimer of AT were achieved using the Gaussian 09 program package[20] without any constraint on the geometry. DFT[21,22] methods along with the three-parameter hybrid functional B3 for the exchange part and the Lee-Yang-Parr (LYP) correlation functional[23-26] was adopted to calculate the properties of the studied molecule. The 6–311++G(d,p) was used as a basis set.

The vibrational frequency assignments of the normal modes were made with a high degree of accuracy, on the basis of the calculated PED with the help of the program GAR2PED[27]. For this purpose a complete set of 150 internal coordinates was defined using Pulay's recommendations[28,29]. GaussView[30] program was used to get the graphical presentation of IR and Raman spectra. For the pictorial visualization and checking of calculated data GaussView and CHEMCRAFT program were used[31].

The electronic parameters, such as highest occupied molecular orbital (HOMO) energy, lowest unoccupied molecular orbital (LUMO) energy and the band gap energy ($\Delta E = \varepsilon_{LUMO} - \varepsilon_{HOMO}$), were obtained through theoretical calculations. Gaussian 09 program using DFT/B3LYP theory was used to perform the NBO and NLO calculation. The NBO analysis was carried out utilizing the

optimized geometry at DFT/B3LYP level using NBO 3.0 program[32] as implemented in Gaussian 09 package in order to understand inter- and intra- molecular delocalization or hyperconjugation.

Molecular electrostatic potential surface (MEP) was plotted for the molecule by the GaussView software. Structure resulting from the plot of electron density surface mapped with electrostatic potential surface depicts the charge density, size, shape and the site of chemical reactivity of a molecule. A detailed analysis of the electron density distribution function was made according to QTAIM suggested by Bader et al.[33-36] using the program AIM2000[37]. Properties of the electron density calculated at bond critical points (BCP) were characterized.

4. Results and discussion

4.1. Geometry Optimizations and Energies

The crystal structure of AT has already been reported by Burley et al.[16] and Boles and Girven[15]. Structural data of Burley et al.[16] have been used to construct the monomer and hydrogen bonded model dimer[16] which are used for further calculations. Initial geometry for both the monomer and the dimer was minimized at DFT level employing B3LYP/6-311++G(d,p). The optimized geometries of monomer and dimer are displayed in Fig. 2 and Fig. 3 respectively. The energy of monomer calculated by DFT (−1714.20 Hartree) is lower than the one calculated by HF (−1705.72 Hartree) showing more stability. The structure of the AT molecule is non-planar.

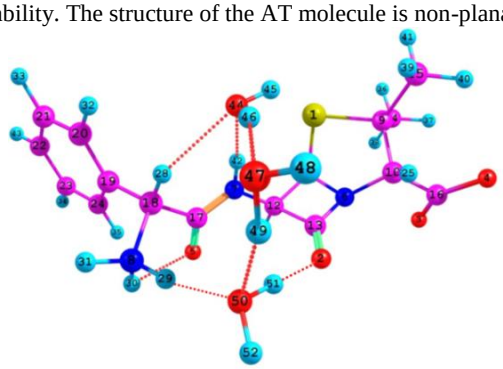

Fig. 2 Optimized structure for monomer of AT and the atom numbering scheme adopted in this study.

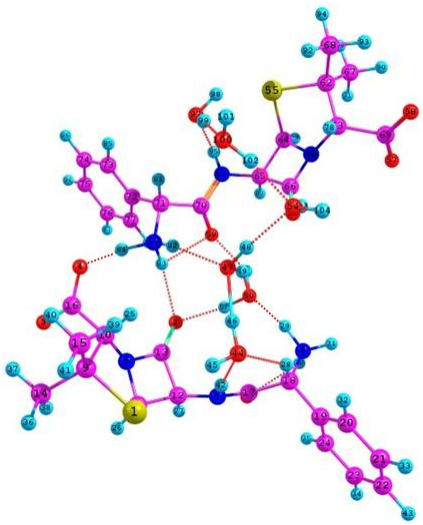

Fig. 3 Optimized structure for dimer of AT and the atom numbering scheme adopted in this study.

The optimized geometrical parameters (bond lengths, bond angles and dihedral angles) of monomer and dimer obtained using DFT methods are listed in Table S1, ESI† and these geometries are compared with the experimental geometry obtained using crystal data of AT[16]. The calculations are capable to reproduce the experimental data within 0.040 Å in bond lengths and 2˚ in bond angles[16]. Significant differences are, however, noticeable in the lengths of S1–C9 bond of the thiazolidine fused ring, N8–C18 bond of the NH_3 group and C10–C16 bond of the COO group where the calculated values are 1.926, 1.525 and 1.597 Å, respectively, as against the experimental values 1.859, 1.475 and 1.555 Å. The bond lengths C20–C21 and C21–C22 at 1.393 Å are indicative of a high degree of π-orbital resonance. In AT the thiazolidine ring atoms form an approximately planar arrangement while the remaining atoms are considerably out of this plane. According to the result in Table S1, some of the bond lengths and angles calculated by DFT methods are somewhat different from the experimental ones, because the molecular states are unlike during theoretical and experimental processes. Only single isolated molecule or dimer is considered in gas phase in theoretical calculation; while many packed molecules are treated in condensed phase in the experimental measurements.

In dimer, many intermolecular hydrogen bonds (H–O···H) are present. The elongation in the bond length of bonds like N7–H42, N8–H29, O47–H48 and O50–H52 from monomer to dimer is the result of strengthening of hydrogen bonds. The total energy of the monomer of AT and its dimer are calculated as −1714.20, −3428.47 a.u., respectively. Therefore, the binding energy of dimer is calculated as 46.65 kcal/mol. The computed binding energy of dimer formation has been rectified for the basis set superposition error (BSSE) by means of the standard counterpoise method[38] and calculated to be 43.89 kcal/mol.

4.2. Chemical reactivity

The chemical reactivity of a molecule can be described in three ways, by using (i) MEP map, (ii) global electronic reactivity descriptors and (iii) molar refractivity (MR).

4.2.1. Molecular electrostatic potential

The MEP explores the polarization and charge transfer effects within the molecule. It also explains hydrogen bonding and reactivity of molecules. This parameter can be used to analyse the electrophilic and nucleophilic sites in the molecule where chemical reactions are expected to take place. It gives a pictorial method to understand the relative polarity of the molecule.

Fig. S1, ESI† and Fig. 4 show the 3D MEP of the monomer and dimer of the title compound, respectively calculated from optimized structure with the electronegative and electropositive regions of the molecule. The different values of the electrostatic potential are symbolized by different colours at the MEP surface; red, blue and green represent the regions of most negative (electrophilic reactivity), most positive (nucleophilic reactivity) and zero electrostatic potential, respectively. Potential decreases in the order blue > green > yellow > orange > red. The colour code of MEP map is in the range between −0.124 a.u. (deepest red) to +0.124 a.u. (deepest blue) and −0.113 a.u. to +0.113 a.u. in monomer and dimer respectively. It may be seen that, in monomer, a region of zero potential covers the π-system of the benzene ring, leaving a more electrophilic region in the plane of the hydrogen atoms. A large electropositive potential is found in the vicinity of the $–NH_3$ group and a small electropositive (blue) region is found near the H_2O molecule in both monomer and dimer. In MEP map of AT the reduction in the electrostatic potential around H_2O molecule indicates the equalization of electrostatic potentials as result of

intramolecular hydrogen bonding H51–O50···H49 and H49–O47···H46. These sites show regions of most positive electrostatic potential and high activity of the NH_3 group. In contrast, areas close to the –COO group shows region of highly electronegative (red) potential and large activity. The region of negative electrostatic potential is linked with the lone pair of electronegative O atoms. The rest of the molecule seems to exert almost neutral electrostatic potential and hence inactive. The same is the case for the dimer of AT.

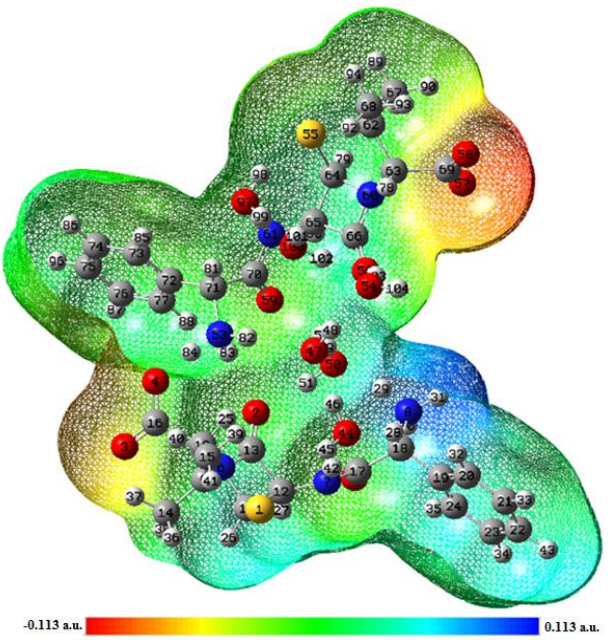

Fig. 4 Molecular electrostatic potential (MEP) formed by mapping of total density over electrostatic potential in gas phase for dimer of AT molecule.

4.2.2. Global reactivity descriptors

According to Koopman's theorem[25], the different global reactivity descriptors, i.e., electronegativity (χ), chemical potential (μ), global hardness (η), global electrophilicity index (ω) and global softness (S) are computed by means of the energies of frontier molecular orbitals ε_{HOMO}, ε_{LUMO} and are given by[39-43];

$$\chi = -\frac{1}{2}(\epsilon_{HOMO} + \epsilon_{LUMO})$$

$$\mu = -\chi = \frac{1}{2}(\epsilon_{HOMO} + \epsilon_{LUMO})$$

$$\eta = \frac{1}{2}(\epsilon_{LUMO} - \epsilon_{HOMO})$$

$$S = \frac{1}{2\eta}$$

$$\omega = \frac{\mu^2}{2\eta}$$

$$\Delta N_{max} = -\frac{\mu}{\eta}$$

According to Parr et al.[40], ω is a global reactivity index resembling with the chemical potential and chemical hardness, which is positive and definite quantity. This ω measures the stabilization in energy when the system gains an additional electronic charge (ΔN) from the surroundings. The electronic chemical potential of the molecule entirely determine the path of the charge transfer as an electrophile is a chemical species proficient of accepting electrons from the surroundings. Hence, its energy must lessen upon accepting electronic charge and its electronic chemical potential must be negative. The energies ε_{HOMO}, ε_{LUMO}, energy band gap (ε_{LUMO}–ε_{HOMO}), χ, μ, η, S and ω for monomer and dimer are listed in Table 1. The calculated high value of ω shows that the monomer behaves as a strong electrophile than dimer.

Table 1 Calculated ε_{HOMO}, ε_{LUMO}, energy band gap (ε_L–ε_H), chemical potential (μ), electronegativity (χ), global hardness (η), global softness (S) and global electrophilicity index (ω) at 298.15 K for monomer and dimer of AT.

Molecule	ε_H (eV)	ε_L (eV)	ε_L–ε_H (eV)	χ (eV)	μ (eV)	η (eV)	S (e/V)	ω (eV)	ΔN_{max}
Monomer	−4.7424	−2.2656	2.4768	3.5040	−3.5040	1.2384	0.4037	4.9572	2.8294
Dimer	−5.0088	−2.2847	2.7241	3.6467	−3.6467	1.3620	0.3671	4.8819	2.6774

4.2.3. Molar refractivity (MR)

MR is an important property used to measure the total polarizability of a mole of a material. It depends on the molecular weight, refractive index and density of the steric bulk and hence responsible for the binding property and lipophilicity of the studied system. It is a constitutive-additive property and may be calculated by the Lorenz-Lorentz formula[44-46]:

$$MR = \left[\frac{n^2 - 1}{n^2 + 2}\right]\left(\frac{MW}{\rho}\right) = 1.333\,\pi N\alpha$$

where n is the refractive index; ρ is the density; MW is the molecular weight; (MW/ρ) is the molar volume; N is the Avogadro number; α is the polarizability of molecular system and its value depends only on the wavelength of the light used to measure 'n'. This equation is usable for both solid and liquid states of the system under study. It is related to the volume of the molecules as well as to the London dispersive forces that act in the drug-receptor interaction. For a radiation of infinite wavelength, the value of MR denotes the real volume of the molecules. The value of MR for monomer and dimer of AT is 53.33 and 134.41 esu, respectively, which are responsible for the binding property of the title molecule and can be used for the cure of different diseases.

4.3. HOMO-LUMO energy gap

There are a number of ways to calculate the excitation energies. The simplest one involves the difference between the HOMO and the LUMO of a neutral system. As they lie at the outermost boundaries of the electrons of the molecules, they are sometimes called the frontier orbitals. They are the main orbitals that take part in chemical stability[47]. The LUMO and HOMO values and their energy gap reflect the biological activity of the molecule. The HOMO as an electron donor represents the ability to donate an electron and LUMO acts as an electron acceptor which accepts an electron. The energy gap between HOMO and LUMO is a critical parameter in determining molecular electrical transport properties because it is a measure of electron conductivity and is mainly

responsible for the chemical and spectroscopic properties of the molecules[48].

The electronic transition of monomer and dimer of AT were calculated in the gas phase using the time dependent (TD)-DFT/6–311++G(d,p) method. The atomic orbital compositions of the molecular orbitals were obtained by GaussView[30]. The features of the HOMO and LUMO of monomer and dimer of AT can be seen in Fig. S2, ESI† and Fig. 5, respectively and their energy gap are found to be 2.4768 eV and 2.7241 eV, respectively. The gap between the HOMO and LUMO determines the electrical transport properties and chemical stability of the molecule[49]. A small gap implies low stability and large gap implies high stability. A molecule with a small HOMO-LUMO gap is more polarizable (reactive), and is generally associated with a high chemical reactivity (less stable)[50-52]. One can also relate the stability of the molecule to hardness, the lower stability indicates that the molecule is softer and chemically more reactive[52]. This is confirmed from Table 1, where the value of global softness (S) is high for monomer and the value of global hardness (η) is high for dimer. So, the chemical reactivity of AT calculated using monomeric model is higher than the one calculated with dimeric model. Our calculations on ampicillin (AMP) show that the HOMO-LUMO gap for AMP is 5.48 eV in comparison to 2.48 eV (monomeric model) for AT[53]. Consequently global reactivity descriptors also indicate that the chemical activity of AT is much higher than AMP.

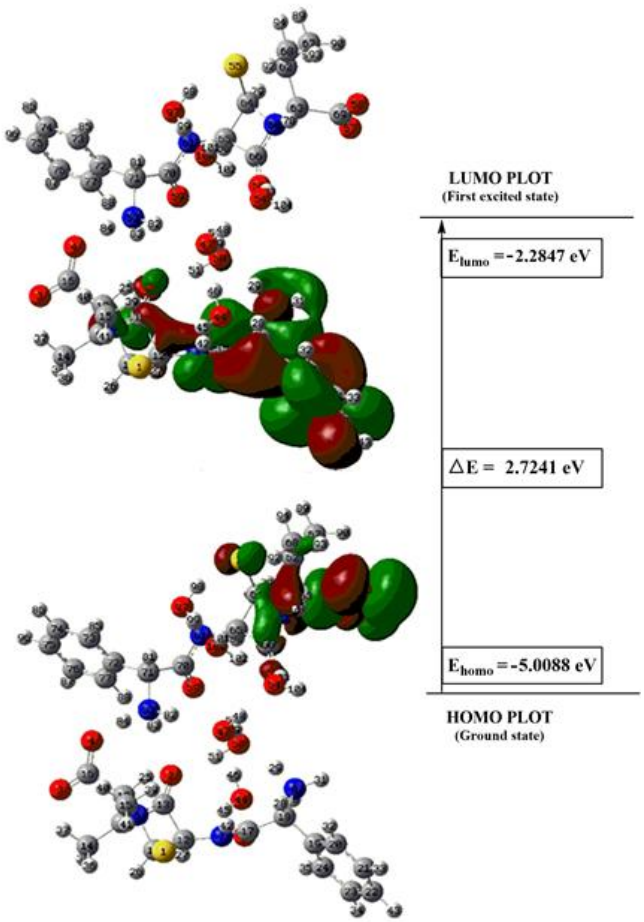

Fig. 5 HOMO-LUMO plot of dimer of AT with orbitals involved in electronic transitions in isolated (gaseous) phase.

The calculated self-consistent field (SCF) energy of AT is −1714.2003 kJ/mol. In HOMO, the charge density is mainly accumulated on the COO group and pentane ring however, in case of LUMO, more charge density moves to the benzene ring and NH_3 group in both, monomer and dimer.

4.4. Natural Bond orbital analysis (NBO)

The NBO analysis has been performed in order to quantifying resonance structure contributions to molecules and also provides an efficient method to study intramolecular charge transfer interactions, rehybridization and delocalization of electron density within the molecule. NBOs are an orthonormal set of localized 'maximum occupancy' orbitals whose leading N/2 members give the most accurate Lewis description of the total electron density[54]. The NBOs are made up of a combination of natural hybrid orbitals (NHOs)[55] which are each made up of an optimized linear combination of natural atomic orbitals (NAOs)[56].

The NBO program is able to provide a complete quantum mechanical description of the structure of a molecule by a set of localized bonds, antibonds and Rydberg extra valence natural atomic orbitals that contribute to the NBOs, lone pair orbitals, etc., including their occupancy and energies. Not only is the analysis able to depict the atomic components of bonding, it is also possible using second order perturbation theory to calculate the strength of interactions such as hydrogen bonds. The larger the value of $E^{(2)}$, the more intensive is the donor-acceptor interaction. Therefore, the $E^{(2)}$ values can be considered a good representation of the bond strength.

NBO analysis of AT was performed to estimate the delocalization patterns of electron density from the principal occupied Lewis-type (bond or lone pair) orbitals to unoccupied non-Lewis (anti-bonding or Rydberg) orbitals. The NBO calculation was performed on the title molecule at the DFT/B3LYP/6–311++G(d,p) level.

For each donor NBO(i) and acceptor NBO(j), the strength of delocalization interaction (or stabilization energy) E(2) associated with electron delocalization between donor and acceptor is estimated by the second order energy lowering as[57,58].

$$E^{(2)} = -n_\sigma \frac{(F_{ij})^2}{E(j) - E(i)}$$

where F_{ij} is the off-diagonal Fock-matrix elements, E(j)−E(i) is the difference in orbital energies of donor and acceptor NBO orbitals and n_σ is the population of the donor orbital. The second- order perturbation theory analyses of the Fock Matrix, in the NBO basis for monomer unit 1 within dimer are presented in Table 2. Overlapping between bonding and anti-bonding orbitals results in intramolecular interactions.

The electron density at the conjugated π bonds (1.64253–1.67406) and π* bonds (0.30786–0.37232) of benzene ring indicate strong π-electron delocalization within ring leading to a maximum stabilization of energy 22.67 kcal/mol. The values of occupancy for σ and π bonding NBOs are 1.96152–1.97622 and 1.64113–1.67537 respectively. The donor ability of π bonding NBOs are much larger than those of σ bonding. The π bonding NBO at C21–C22 has lowest occupancy 1.64113, hence possesses the strongest donor ability among all the bonding NBOs. Likewise, larger occupancies of the antibonding NBOs lead to the stronger acceptor ability.

An important interaction, related to the resonance in the molecule is the electron donation from oxygen atom n3(O4) to π*O3–C16 leading to high stabilization energy of 75.31 kcal/mol,

this larger energy shows the hyperconjugation within the COO group. While the atoms n(2)O2 and n(2)O5 share the energies of 23.35 and 22.69 kcal/mol to σ*N6–C13 and σ*N7–C17 bonds respectively.

Table 2 Second order perturbation theory analysis of the Fock matrix in the NBO basis for intramolecular interactions for monomer unit 1 within dimer of AT.

Donor NBO (i)	ED(i) (e)	Acceptor NBO (j)	ED(j) (e)	E(2)[a] (kcal/mol)	E(j)−E(i)[b] (a.u.)	F(i,j)[c] (a.u.)
within unit 1						
σN6–C11	1.97106	σ*O2–C13	0.02999	7.82	1.27	0.089
σN7–H42	1.97622	σ*O5–C17	0.01503	5.69	1.23	0.075
σC11–C12	1.97043	σ*O2–C13	0.02999	6.46	1.19	0.078
σC12–C13	1.96152	σ*N6–C10	0.04560	5.92	0.94	0.067
σC14–H37	1.97412	σ*S1–C9	0.06939	6.27	0.58	0.054
σC15–H40	1.97588	σ*S1–C9	0.06939	5.86	0.59	0.053
πC19–C20	1.67537	σ*N8–C18	0.03766	6.92	0.47	0.055
		π*C21–C22	0.30687	17.92	0.29	0.065
		π*C23–C24	0.30856	19.98	0.29	0.068
πC21–C22	1.64113	π*C19–C20	0.37293	22.67	0.27	0.070
		π*C23–C24	0.30856	20.01	0.28	0.068
πC23–C24	1.65566	π*C19–C20	0.37293	20.97	0.28	0.068
		π*C21–C22	0.30687	19.85	0.29	0.068
n(2)S1	1.92166	σ*C11–H26	0.03671	5.09	0.65	0.052
n(2)O2	1.84380	σ*N6–C13	0.06724	23.35	0.75	0.121
		σ*C12–C13	0.08722	20.78	0.60	0.102
n(2)O3	1.85678	σ*O4–C16	0.06388	22.22	0.76	0.118
		σ*C10–C16	0.12084	23.22	0.55	0.101
n(1)O4	1.94364	σ*C10–C16	0.12084	8.43	0.86	0.077
n(2)O4	1.85139	σ*O3–C16	0.03761	14.63	1.02	0.112
n(3)O4	1.64981	π*O3–C16	0.31079	75.31	0.29	0.134
n(2)O5	1.86094	σ*N7–C17	0.06543	22.69	0.75	0.119
		σ*C17–C18	0.07682	20.89	0.60	0.101
n(1)N6	1.65273	π*O2–C13	0.31131	48.31	0.30	0.109
n(1)N7	1.66172	π*O5–C17	0.32238	66.06	0.27	0.121
		σ*C12–C13	0.08722	7.79	0.60	0.065
π*C19–C20	0.37293	π*C21–C22	0.30687	288.76	0.30	0.083

[a]E(2) means energy of hyperconjugative interaction (stabilization energy).
[b]Energy difference between donor (i) and acceptor (j) NBO orbitals.
[c]F(i, j) is the Fock matrix element between i and j NBO orbitals.

Table 3 Second order perturbation theory analysis of the Fock matrix in the NBO basis for the intermolecular interactions for dimer of AT.

Donor NBO (i)	ED(i) (e)	Acceptor NBO (j)	ED(j) (e)	E(2)[a] (kcal/mol)	E(j)−E(i)[b] (a.u.)	F(i,j)[c] (a.u.)
from unit 1 to unit 4						
n(1)O2	1.96119	σ*O50–H51	0.02984	5.79	1.15	0.073
n(2)O2	1.84380	σ*O50–H51	0.02984	5.85	0.73	0.060
from unit 2 to unit 1						
n(2)O44	1.95508	σ*N7–H42	0.05554	16.26	0.83	0.104
from unit 3 to unit 2						
n(2)O47	1.95639	σ*O44–H46	0.03674	16.29	0.82	0.104
from unit 4 to unit 1						
n(2)O50	1.92811	σ*N8–H29	0.07242	31.35	0.88	0.149
from unit 4 to unit 3						
n(1)O50	1.98150	σ*O47–H49	0.01441	5.21	0.85	0.059
from unit 5 to unit 6						
n(1)O56	1.96324	σ*O54–H103	0.04318	6.53	1.12	0.076
n(2)O56	1.84597	σ*O54–H103	0.04318	7.65	0.70	0.067
from unit 6 to unit 3						
n(1)O54	1.97582	σ*O47–H48	0.02225	7.59	0.80	0.070
from unit 6 to unit 7						
n(1)O54	1.97582	σ*O97–H99	0.02780	16.09	2.36	0.174
from unit 6 to unit 8						
σO54–H103	1.99643	σ*O100–H101	0.00075	99.68	3.28	0.510
		σ*O100–H102	0.02451	91.22	3.03	0.472
σO54–H104	1.99746	σ*O100–H101	0.00075	264.53	3.24	0.826
		σ*O100–H102	0.02451	91.59	2.99	0.470

n(1)O54	1.97582	σ*O100–H101	0.00075	13.41	2.87	0.176
		σ*O100–H102	0.02451	12.59	2.63	0.162
n(2)O54	1.97193	σ*O100–H101	0.00075	175.83	3.14	0.668
		σ*O100–H102	0.02451	9.55	2.89	0.148
from unit 7 to unit 5						
n(2)O97	1.95404	σ*N61–H95	0.05788	16.73	0.83	0.105

The second-order perturbation theory analyses of the Fock Matrix, in the NBO basis for dimer of AT are presented in Table 3. In dimer, total 8 units are present, charge transfer from unit (6) to unit (9) due to n(1)O54/n(2)O54→σ*O100–H101 stabilized the molecule up to 175.83 kcal/mol and confirms the presence of classical interaction O100–H101···O54. In the same way, intermolecular charge transfer n(1)O54/n(2)O54→σ*O100–H102 confirms the presence of classical interaction O100–H102···O54. Another weak intermolecular charge transfer from monomer unit (1) to unit (4) due to n(1)O2/n(2)O2→σ*O50–H51 confirms the presence of intermolecular interaction O50–H51···O2 and stabilized the molecule up to 5.85 kcal/mol.

Selected Lewis orbitals (occupied bond orbital) for monomer of AT with percentage ED over bonded atoms (ED_X, ED_Y in %), hybrid NBOs with s and p character are listed in Table S2, ESI†. The valence hybrids analyses of NBOs show that all the C–N and C–O bond orbitals are polarized towards the nitrogen (73.09% at N), oxygen (62.23% at O) atoms, however the C–S bond orbitals are polarized towards the sulphur atom (85.09% at S). The electron density distribution (occupancy) about the NH_3 group mainly affects the polarity of the compound. Consequently, they consist with the maximum electron density on the oxygen, nitrogen and sulphur atom and responsible for polarity of the molecule.

4.5. Static dipole moment (μ), mean polarizability (α_0), anisotropy of polarizability (Δα) and first hyperpolarizability (β_0)

Non Linear Optical (NLO) phenomena have been widely studied over the last decades. Molecules showing large hyperpolarizabilities have a strong NLO potential and could be used, under conditions, for optoelectronics and a variety of optical devices. Theoretical determination of hyperpolarizability is moderately useful in understanding the relationship between the molecular structure and NLO properties. It helps in designing and synthesizing organic NLO materials. Computational calculation is used to measure hyperpolarizability as it is difficult to measure it directly.

NLO parameters static dipole moment (μ), mean polarizability (α_0), anisotropy of polarizability (Δα) and first hyperpolarizability (β_0) are calculated using following equations[59]:

$$\mu = \left(\mu_x^2 + \mu_y^2 + \mu_z^2\right)^{1/2}$$

$$\alpha_0 = \frac{1}{3}\left(\alpha_{xx} + \alpha_{yy} + \alpha_{zz}\right)$$

$$\Delta\alpha = 2^{-1/2}\left[\left(\alpha_{xx} - \alpha_{yy}\right)^2 + \left(\alpha_{yy} - \alpha_{zz}\right)^2 + \left(\alpha_{zz} - \alpha_{xx}\right)^2\right]^{1/2}$$

$$\beta = \left(\beta_x^2 + \beta_y^2 + \beta_z^2\right)^{1/2}$$

where

$$\beta_x = \beta_{xxx} + \beta_{xyy} + \beta_{xzz}, \beta_y = \beta_{yyy} + \beta_{yzz} + \beta_{yxx}, \beta_z = \beta_{zzz} + \beta_{zxx} + \beta_{zyy}$$

The values of μ, α_0, Δα and β_0 of monomer and dimer of AT are listed in Table S3, ESI†. The components of α and β_0 are reported in atomic units and the calculated values are converted into electrostatic units (For α: 1 a.u. = 0.1482×10^{-24} esu; for β_0: 1 a.u. = 8.639×10^{-33} esu). Organic NLO materials have many advantages over inorganic materials, such as large nonlinear optical coefficients, simple preparation, greater ease for synthetic design and lower cost[60-62]. Organic materials are frequently formed by weak van der Waals and hydrogen bonds and hence possess a high degree of de1ocalization. AT is an interesting material for NLO application as it contains a proton acceptor (deprotonated) carboxylic acid group (COO) and the proton donor amino group (NH_3). The β_0 values for monomer and dimer are calculated as $8.12345*10^{-30}$ and $7.28859*10^{-30}$ esu. Here, para-nitoaniline (p-NA) is chosen as a reference molecule (for p-NA, $\beta_0 = 14.26*10^{-30}$ esu)[63]. Therefore, the calculated results show that the titled molecule might have good NLO response.

4.6. Thermodynamic properties

Enthalpy (H°_m), heat capacity ($C^\circ_{p,m}$) and entropy (S°_m), all these thermodynamic properties, are important parameters in predicting reactive properties of chemical reactions. On the basis of statistical thermodynamics and vibrational analyses, these parameters were obtained for monomer (given in Table S4, ESI†). As observed from this table, the values of these parameters increase with the increase of temperature from 100 K to 500 K which is attributed to the enhancement of molecular vibration while the temperature increases. The correlation between these thermodynamic properties and temperatures are shown in Fig. 6. The correlation equations for monomer of AT are as follows:

$H^\circ_m = Y = 261.41787 + 0.02497\ T + 1.4436 \times 10^{-4}\ T^2$ ($R^2 = .99995$)

$S^\circ_m = Y = 12.65204 + 0.38447\ T - 1.6366 \times 10^{-4}\ T^2$ ($R^2 = 0.99989$)

$C^\circ_{p,m} = Y = 66.00334 + 0.50456\ T - 1.88983 \times 10^{-4}\ T^2$ ($R^2 = .99993$)

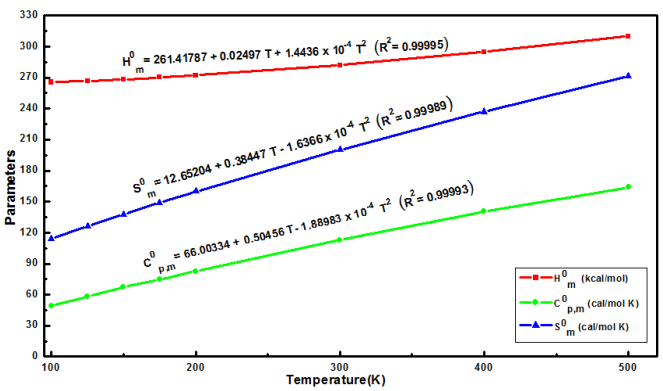

Fig. 6 Correlation graphics of thermodynamic properties and temperature for monomer of AT.

All these correlation equations might be used for the advance studies on the title compound. As, when the interaction of AT with another compound is studied, these thermodynamic properties might be obtained from these equations. These equations can be used to determine the change in Gibbs free energy of the reaction, which will consecutively help to judge the spontaneity of the reaction.Zero-point energies, entropies (S), heat capacities (C), enthalpies (H), Gibbs free energies (G), all these thermodynamic parameters at room temperature (298.15 K) for monomer and dimer of AT are presented in Table S5, ESI†.

The calculated enthalpy (H), Gibbs free energy (G), entropy (S), their change and equilibrium constant (K_{eq}) of conversion from monomer to dimer at 25 ˚C are listed in Table 4. The reaction has negative values for ΔH, and ΔG specifying that the reaction is exothermic and spontaneous at room temperature. Thermodynamic relation between ΔG and K_{eq} at temperature (T) is given as $K_{eq} = e^{-\Delta G/RT}$. Using this relation, K_{eq} for the reaction is calculated as $1.32*10^9$ at room temperature. This specifies that the dimer formation will be preferred at room temperature.

Table 4 The thermodynamic quantities (enthalpy, Gibbs free energy, entropy), their change and equilibrium constant of conversion from monomer to dimer.

Parameters	Enthalpy (H) (kcal/mol)	Gibbs free energy (G) (kcal/mol)	Entropy (S) (cal/mol K)	ΔH (kcal/mol)	ΔG (kcal/mol)	ΔS (cal/mol K)	K_{eq}
2xMonomer	−2150790.52	−2150909.75	398.672	−43.92	−12.55	−44.914	$1.32*10^9$
Dimer	−2150834.45	−2150922.30	353.758				

4.7. Atoms in molecules (AIM) calculations

In order to have an insight into a region of a system, QTAIM method has been applied. Geometrical and topological parameters are very helpful means to illustrate the strength of hydrogen bond. The point on the bond path with the lowest value of the electron density (minimum along the path) is the bond critical point (BCP). The geometrical conditions for the occurrence of hydrogen bond are based on: (i) the distance between proton (H) and acceptor (A) is less than the sum of their van der Waal's radii. (ii) The 'donor (D)–proton (H)····acceptor (A)' angle is greater than 90̊. (iii) The elongation of 'D–H' bond length is observed.

As the above conditions are recurrently considered as inadequate, the existence of hydrogen bond could be supported further by Koch and Popelier criteria[64] based on 'Atoms in Molecules' theory (i) The existence of bond critical point for the 'H····A' contact as a confirmation of the existence of hydrogen bonding / interaction (ii) The value of electron density ($\rho_{H\cdots A}$) should be within the range 0.0020–0.0400 a.u. (iii) The corresponding Laplacian ($\nabla^2\rho_{BCP}$) should be within the range 0.024–0.139 a.u. if hydrogen bond exist. According to Rozas et al.[65] the H-bond interactions may be classified as follows: (i) Strong H bonds are categorized by ($\nabla^2\rho_{BCP}$) < 0 and H_{BCP} < 0 and their covalent character is established, (ii) Medium H-bonds are categorized by ($\nabla^2\rho_{BCP}$) > 0 and H_{BCP} < 0 and their partially covalent character is established and (iii) Weak H-bonds are categorized by ($\nabla^2\rho_{BCP}$) > 0 and H_{BCP} > 0 and they are mostly electrostatic in nature and the distance between interacting atoms is less than the sum of their van der Waal's radii.

$\nabla^2\rho(r_{BCP})$ is related to the energy of bond interaction by the expression of the virial theorem.

$$1/4\ \nabla^2\rho(r_{BCP}) = 2G(r_{BCP}) + V\rho(r_{BCP}) = H(r_{BCP})$$

where $G(r_{BCP})$ is the kinetic energy density, $\rho(r_{BCP})$ the electron density, $H(r_{BCP})$ the total electron density and $V(r_{BCP})$ potential energy density at bond critical point (BCP).

Table 5 Geometrical parameter (bond length) and topological parameters for bonds of interacting atoms of dimer: electron density (ρ_{BCP}), Laplacian of electron density ($\nabla^2\rho_{BCP}$), electron kinetic energy density (G_{BCP}), electron potential energy density (V_{BCP}), total electron energy density (H_{BCP}) at bond critical point (BCP) and estimated interaction energy (E_{int}).

Interactions	Bond length (Å)	ρ_{BCP} (a.u.)	$\nabla^2\rho_{BCP}$ (a.u.)	G_{BCP} (a.u.)	V_{BCP} (a.u.)	H_{BCP} (a.u.)	E_{int} (kcal/mol)
O4····H84	1.45584	0.08646	0.13642	−0.03095	−0.09600	−0.12695	−30.12048
O50····H29	1.64932	0.05223	0.14184	−0.00743	−0.05031	−0.05774	−15.78188
O56····H103	1.71339	0.04131	0.13701	−0.00198	−0.03822	−0.04020	−11.99172
O47····H46	1.78743	0.03679	0.11862	−0.00090	−0.03145	−0.03235	−9.85879
O2····H51	1.79480	0.03329	0.11998	−0.00074	−0.02851	−0.02925	−8.94202
O100····H99	1.80834	0.03305	0.11779	−0.00073	−0.02799	−0.02799	−8.77886
O97····H95	1.85386	0.03282	0.10459	−0.00013	−0.02588	−0.02601	−8.11998
O44····H42	1.87066	0.03202	0.10210	−0.00027	−0.02498	−0.02525	−7.83760
O54····H102	1.84473	0.03052	0.10996	−0.00127	−0.02494	−0.02621	−7.82505
O59····H52	1.89351	0.02668	0.10275	−0.00197	−0.02174	−0.02371	−6.82104
O54····H48	1.88965	0.02748	0.09849	−0.00156	−0.02151	−0.02307	−6.74573
O50····H49	2.06313	0.01969	0.06715	−0.00171	−0.01337	−0.01508	−4.19177
O47····H82	2.11576	0.01839	0.06026	−0.00165	−0.01176	−0.01341	−3.68976
O2····H83	2.11771	0.01754	0.06370	−0.00215	−0.01163	−0.01378	−3.64583
O3····H37	2.49185	0.01201	0.04322	−0.00145	−0.00791	−0.00936	−2.47866
O44····H28	2.33303	0.01217	0.04189	−0.00151	−0.00745	−0.00745	−2.33434
S55····H98	2.57355	0.01441	0.03743	−0.00106	−0.00723	−0.00829	−2.26531
O5····H35	2.55309	0.00958	0.03200	−0.00101	−0.00597	−0.00698	−1.86998
O97····H81	2.48948	0.00917	0.03048	−0.00104	−0.00553	−0.00657	−1.73193
O59····H88	2.65897	0.00814	0.02845	−0.00099	−0.00513	−0.00612	−1.60643

The molecular graph of monomer and dimer of AT using AIM program at B3LYP/6–311++G(d,p) level is shown in Fig. S3, ESI† and Fig. 7. Topological, geometrical and energy parameters for intermolecular hydrogen bonds of interacting atoms are listed in Table 5. The geometrical parameters for hydrogen bonds in dimeric model of AT are given in Table S6, ESI†. On the basis of these parameters, O47····H46, O44····H42 and O50····H49, O44····H28, O5····H35, S1····H45, O4····H40, etc. all are medium hydrogen bonds. In this article, the QTAIM theory is used to estimate hydrogen bond energy (E). The proportionality between E and V_{BCP} at H···O contact is $E = 1/2(V_{BCP})$[66]. The calculated interaction energy at BCP indicates that three inter molecular H-bonding O4····H84, O50····H29 and O56····H103 are strong however, O47····H46, O2····H51, O100····H99, O97····H95, O44····H42, O54····H102, O59····H52, O54····H48 and O50····H49 are moderate in nature, whereas rests are weaker interactions.

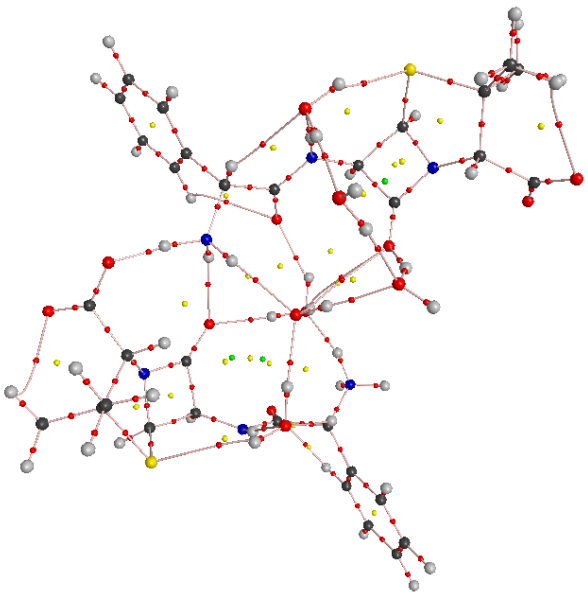

Fig. 7 Molecular graph of dimer of AT: bond critical points (small red spheres), ring critical points (small yellow sphere), bond paths (pink lines).

4.8. Vibrational assignments

The AT comprises of 52 atoms, which has 150 (3n−6) vibrational degrees of freedom and dimer of AT have 306 degrees of freedom. No special symmetry was found in the molecular conformation obtained from the crystalline structure, as well as yielded by geometry optimization. All the 150 fundamental vibrations are both IR and Raman active.

DFT calculations yield Raman scattering amplitudes which cannot be taken directly to be the Raman intensities. The Raman scattering cross-sections, $\partial\sigma_j/\partial\Omega$, which are proportional to the Raman intensities may be calculated from the Raman scattering amplitude and predicted wavenumbers for each normal modes using the relationship[67,68]:

$$\frac{\partial\sigma_j}{\partial\Omega} = \left(\frac{2^4\pi^4}{45}\right)\left(\frac{(\nu_0-\nu_j)^4}{1-\exp\left[\frac{-hc\nu_j}{kT}\right]}\right)\left(\frac{h}{8\pi^2 c\nu_j}\right)S_j$$

where S_j and σ_j are the scattering activities and the predicted frequencies (in cm^{-1}), respectively of the j^{th} normal mode, ν_0 is the Raman exciting frequency (in cm^{-1}), and h, c and k are universal constants.

The scaled IR and Raman intensities and wavenumbers were computed with Lorentzian line shape (FWHM = 8 cm^{-1}). Assignments are made on the basis of relative intensities, energies, line shape and PED. PED values less than 5% have not been incorporated in the Table S7, ESI†. Fig. 8 and Fig. 9 present a comparison of the experimental and theoretically predicted infrared spectra in the 600–3750 cm^{-1} region and the corresponding Raman spectra in the 100–3750 cm^{-1} region, for monomer, dimer, respectively. A reasonable agreement has been obtained in the frequencies and intensities of the observed and theoretical spectra.

4.9. Vibrational wavenumbers

The absolute Raman scattering and infrared absorption intensities associated with each normal mode, were calculated in the harmonic approximation at the same level of theory as used for the optimized geometries. It is to be noted that the DFT vibrational wavenumbers are known to be higher than the experimental wavenumbers; they were scaled down by the wave number linear scaling procedure (WLS)[69] by using the relation:

$$\upsilon_{obs} = (1.0087-0.0000163\upsilon_{cal})\,\upsilon_{cal}\ cm^{-1}$$

The calculated values of the Raman and IR wavenumbers and intensities of vibrational bands and PED of the AT and predicted modes for the dimer, together with the observed frequencies are tabulated in Table S7.

4.9.1. C–NH_3 group vibrations

The symmetric and asymmetric stretching modes of NH_3 group for monomer are calculated to be 3233 and 3345 cm^{-1}, respectively corresponding to the observed IR peaks at 3207 cm^{-1} and 3367 cm^{-1}. The same symmetric and asymmetric modes in dimer are predicted at 3186 and 3247 cm^{-1}, respectively. In monomer as well as dimer one of the hydrogen atoms of NH_3 group (H29) is hydrogen bonded with oxygen atom (O50) of water molecule. The stretching mode of N–H29 bond in dimer leads to an 87 cm^{-1} downshift corresponding to a small increase in N –H bond length of 0.008 Å. The N–H29 stretching mode is observed at 2754/2742 cm^{-1} in the Raman/IR spectra respectively.

4.9.2. Benzene ring vibrations

The substituted benzene ring is abbreviated as R3. In literature, the aromatic C–H stretching vibrations, out-of-plane C–H bending and ring bending vibration in substituted benzene rings are reported in the region 3000–3100, 900–675, 600–420 cm^{-1}, respectively[70]. In R3, the observed C–H stretching mode at 3039/3045 cm^{-1} in the IR/Raman corresponds to the calculated wavenumber at 3059/3056 cm^{-1} in monomer/dimer.

The organic compounds having aromatic hydrocarbons commonly exhibit multiple weak bands in the region 1600–1585 cm^{-1} and 1500–1400 cm^{-1} due to C–C stretching vibrations[70]. The C–C stretching mode predicted at 1595 cm^{-1} corresponds to well define peaks at 1606 cm^{-1} in the IR spectrum and at 1594 cm^{-1} in the Raman spectrum. The C–H in-plane bending modes are observed at 1334 and 1169 cm^{-1} in the IR spectrum, 1337 and 1177 cm^{-1} in the Raman spectra match well with the calculated modes at 1339 and 1176 cm^{-1}. IR bands at 1020, 989, 972 and 875 cm^{-1} and its counterpart at 1024, 993, 965 and 880 cm^{-1}in the Raman spectrum are assigned to the out-of-plane bending of CH group. These modes are calculated at 1014, 994, 960 and 863 cm^{-1}.

4.9.3. Ring 2 vibrations

The stretching mode of β-lactam ring R2 [υ(CH)] calculated at wavenumber 2997 cm^{-1} in monomer as well as dimer corresponds to

the observed band at 2996/2991 cm^{-1} in the Raman/IR spectrum. Oxygen atom of C=O group is hydrogen bonded with hydrogen atom (H51) of water molecule in both monomer and dimer. The computed C=O stretch mode in monomer at 1729 cm^{-1} show a blue shift in dimer and occurs at 1745 cm^{-1}. A small decrease of 0.008 Å in the bond length of C=O occurs because of this upshift in wavenumber from monomer to dimer. A very strong band in IR and weak band in Raman spectrum at 1572 and 1594 cm^{-1} are assigned to NH rocking mode. The theoretical computed wavenumber for this mode is at 1579 cm^{-1} for both monomer and dimer. The stretching mode of CN bond is calculated to be 1403 cm^{-1} and assigned to the peak at 1405/1402 cm^{-1} in the Raman/IR spectrum.

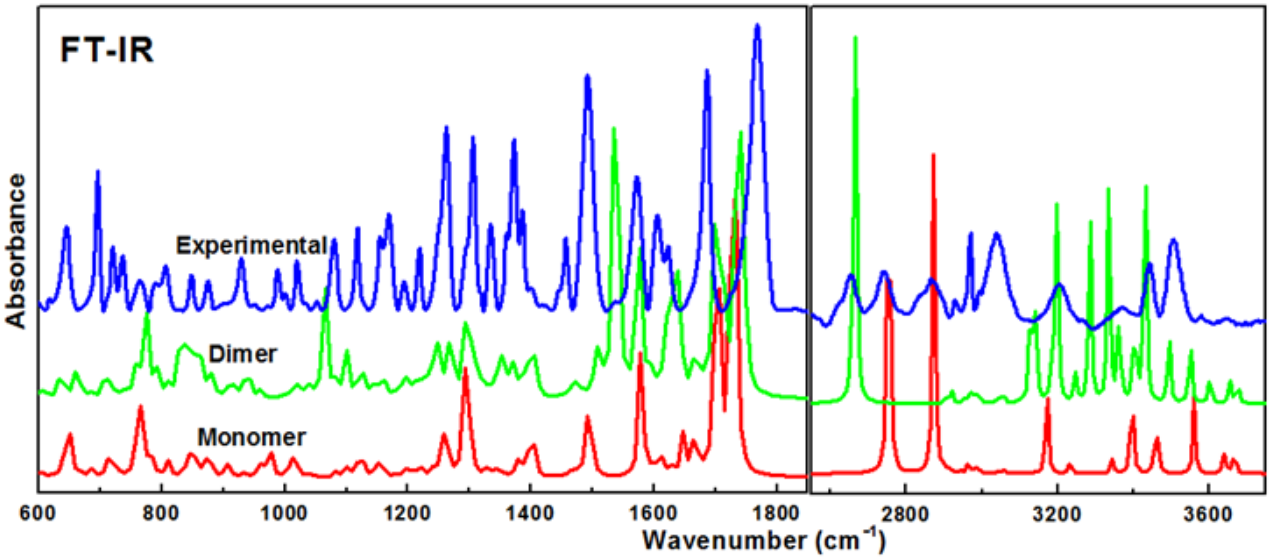

Fig. 8 Observed and calculated (scaled) FT-IR absorbance spectra of AT in the region, 600–1850 cm^{-1} and 2550–3750 cm^{-1}.

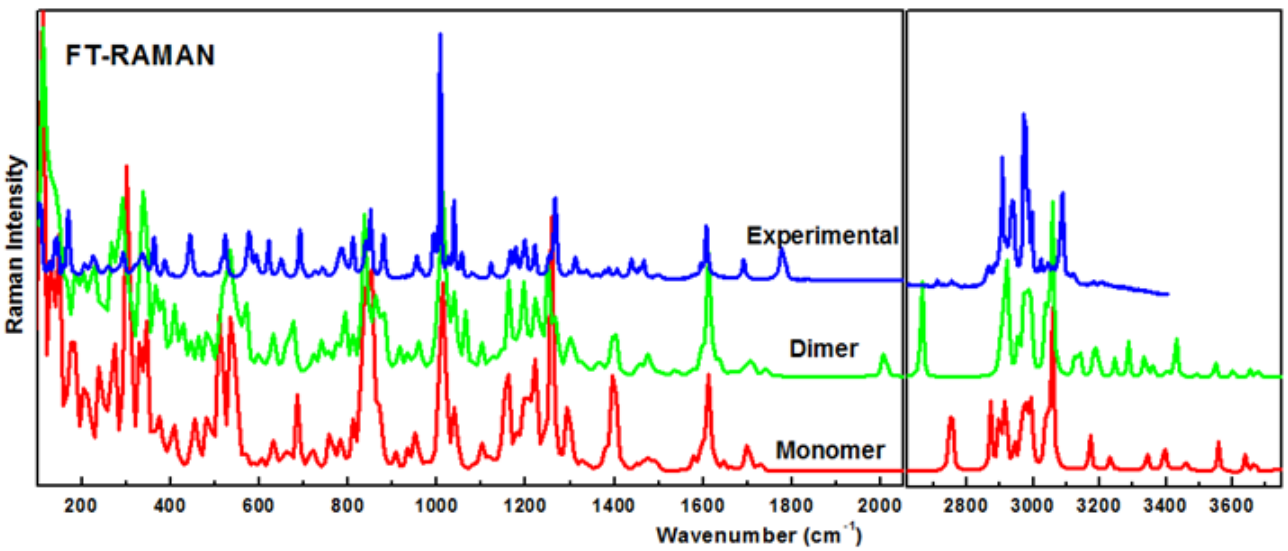

Fig. 9 Observed and calculated (scaled) Raman scattering spectra of AT in the region, 100–2050 cm^{-1} and 2620–3750 cm^{-1}.

4.9.4. Ring 1 vibrations

The C–H stretching modes of thiazolidine ring are calculated at 2944 and 2974 cm^{-1} corresponding to a weak IR band at 2929 cm^{-1} and strong Raman bands at 2939 and 2976 cm^{-1}. The CCH wagging motions are calculated to be at 1348 cm^{-1}corresponding to the observed strong IR band at 1361 cm^{-1}. The CCH deformation is computed at 1243 cm^{-1} and occurs at 1263/1252 cm^{-1} in the recorded IR/Raman spectrum. The C–C stretching modes are calculated to be 951/843 cm^{-1} corresponding to the observed strong Raman band 955/841 cm^{-1} and IR peak at 951/843 cm^{-1}. Ring deformation and CC rocking motions are calculated to be 512/379 cm^{-1} and matches well with the experimental values.

The asymmetric and symmetric stretching modes of CO_2 group attached to R1 are calculated to be 1703 and 1295 cm^{-1} respectively. Asymmetrical and symmetric stretching of this group appears at 1691 and 1298 cm^{-1} in Raman spectra and at 1685 and 1306 cm^{-1} in the IR spectrum.

4.9.5. C–CH_3 group vibrations

The monomer of AT possesses two methyl groups, the symmetric and asymmetric stretching of the $C14H_3$ group occurs at

2935/2929 cm^{-1} and at 2985/2991 cm^{-1} in the Raman/IR spectrum, respectively and these modes are calculated to be 2916 and 2987 cm^{-1}. Similarly the symmetric and asymmetric C–H stretching vibrations of the $C15H_3$ group are calculated at 2900 and 2970 cm^{-1} respectively which is in good agreement with the observed band at 2907 cm^{-1} in the Raman spectra and 2970/2971 cm^{-1} in the IR/Raman spectra. Mixed asymmetric deformation mode is calculated to be 1452, 1468, 1473 and 1487 cm^{-1} with contributions from $C14H_3$ and $C15H_3$ groups appear at 1438/1458 cm^{-1} and 1466/1493 cm^{-1} in Raman/IR spectrum. Symmetric deformation mode of $C14H_3$ group is assigned to the IR peak at 1402 and Raman peak at 1405 cm^{-1} respectively and is calculated at 1403 cm^{-1}. It is a mixed mode containing the contribution from C–N stretching. The symmetric $C15H_3$ deformation vibration is calculated to be 1376 cm^{-1} and matches well with the IR and Raman wavenumbers. It is also a mixed mode containing the contribution from $C14H_3$ deformation.

4.9.6. Amide group vibrations

In the FT-IR spectrum of AT, the N–H stretch is observed at 3207 cm^{-1}, whereas it is calculated as 3172 and 3139 cm^{-1} in monomer and dimer , respectively. This downshift in the wavenumber from monomer to dimer is attributed to the increase in the bond length of N –H from monomer to dimer by 0.002 Å due to strong intermolecular N–H···O interaction in dimer. The broadening of the N–H peak occurs due to the overlapping of NH_3 group peaks. The observed NH rocking mode at 1572 cm^{-1} in the IR spectra is in agreement with the calculated wavenumber at 1579 cm^{-1} in monomer as well as dimer. The observed N7–H wagging mode at 737 cm^{-1} corresponds to the calculated wavenumber at 757 cm^{-1}.

The strong IR band observed at 1685 cm^{-1} and its Raman counterpart at 1691 cm^{-1} are assigned to the C=O stretching mode and calculated at 1701 and 1705 cm^{-1} in monomer and dimer. It is a mixed mode having contribution from C17–N stretching also.

4.9.7. H_2O vibrations

In AT each ampicillin molecule is attached to three water molecules. Here most of the O–H bonds of water molecules are involved in hydrogen bonding. In the literature the free O–H stretching mode occurs in the range 3530–3645 cm^{-1} whereas the hydrogen bonded O–H mode is observed in the range 3200–3570 cm^{-1}[171]. The computed O44–H46 stretch mode in monomer at 3560 cm^{-1} shows a red shift in dimer and occurs at 3286 cm^{-1}. This downshift in the wavenumber corresponds to an increase in O –H bond length, which is 0.977 Å in monomer and 0.983 Å in dimer. The O47····H46–O44 hydrogen bond is strongest among all the H–bonds as O44–H46 bond length turn out to be longest among all the O–H bonds in dimer. Similarly O47–H49 stretching mode also show a red shift where this stretching occurs at 3666 cm^{-1} in monomer and at 3492 cm^{-1} in dimer with a raise of bond length from monomer to dimer by 0.004 Å. In the observed FT-IR spectrum of AT (Fig. 8), the characteristic peak corresponding to the stretching mode of the OH group is identified at 3442 and 3506 cm^{-1}. The stretching modes O–H of the second molecule in dimer are calculated at 3675, 3656 and 3549 cm^{-1}. The O–H wagging mode calculated at 786 cm^{-1} corresponds to the observed band at 791 cm^{-1} in the IR spectra and at 783 cm^{-1} in the Raman spectra.

5. Conclusions

The structural and hydrogen bonding features are discussed combining spectroscopic, density functional theory (DFT) and quantum theory of atoms in molecules (QTAIM) results on monomer and dimer of ampicillin trihydrate (AT). Attempts have been made for the proper wavenumber assignments for the FT-IR and FT-Raman spectra. The vibrational bands observed in both these spectra were assigned and supported by theoretically calculated (scaled) DFT vibrational spectra. The optimized geometrical parameters of the dimer were compared with that of the monomer. The significant changes in bond lengths of the monomer upon dimerization were explained. The calculated OH stretching mode of H_2O agrees better in dimer than in the monomer. Intermolecular hydrogen bonding between water molecules and N–H and C=O groups, and subsequent changes in vibrational wavenumbers and bond lengths of O–H group involved in hydrogen bonding were discussed. The nucleophilic and electrophilic sites on the molecular electrostatic potential surface were determined. HOMO–LUMO calculations were performed on the monomer and the dimer of AT. Parameters describing chemical reactivity of AT, in addition to HOMO–LUMO and MEP surfaces have been used to explain electronic properties. It has been theoretically established that AT is chemically more active than ampicillin (AMP), due to smaller HOMO–LUMO gap, less chemical hardness as well as enhanced hydrogen bonding properties. The natural bond orbital (NBO) result reflects the charge transfer in the molecule. The value of first hyperpolarizability (β_0 = 8.12345*10^{-30} esu) shows that AT has potential to be used for non-linear optical (NLO) applications. QTAIM calculations suggest that the nature of the hydrogen bonds present in the title molecule is moderate due to $(\nabla^2\rho_{BCP}) > 0$ and $H_{BCP} < 0$. The present study may suggest that it can be possible to design a new series of drugs with suitable substitution with increased biological and chemical activity.

Acknowledgements

We are thankful to Dr. M.C. Gamberini, Institute of Pharmacy, University of Modena and Reggio Emilia, Italy, for providing the sample. P.Tandon, E.Khan, Shweta and A.Srivastava are thankful to UGC, New Delhi for providing financial assistance under UGC research award, UGC-BSR fellowship, UGC-RGN fellowship and PDF for Women Scientist, respectively. A.Shukla acknowledges the financial support provided by the DST, India under the DST-PURSE fellowship.

Notes and references

[a] Department of Physics, University of Lucknow, Lucknow 226 007, India

* Corresponding author. Tel.: +91 522 2782653; fax: +91 522 2740840. E-mail addresses: poonam_tandon@yahoo.co.uk, poonam_tandon@hotmail.com. (P. Tandon).

† Electronic Supplementary Information (ESI) associated with this article can be found, in the online version, at http://dx.doi.org/10.1039/b000000x/

1 R. Greek, L. A. Hansen, Biological Systems, Vol 2, Issue 2 (2013)
2 The discovery and development of penicillin, Royal Society of Chem., American Chemical Society (1999)
3 A. Fleming, Brit. J. Exptl. Pathol., 10, 226 (1929).
4 B. A. Cunha, Urology 40 (2) (1992)186–90.
5 IARC Monographs on the Evaluation of Carcinogenic Risks to Humans, Vol. 50, (1990) 153−167.
6 K.W.B. Austin, A.C. Marshall, H. Smith, Nature 208 (1965) 999.
7 M.N.G. James, D. Hall, Nature 220 (1968) 168.
8 J.W. Poole, C.K. Bahal, J. Pharm. Sci. 57 (1968) 1945.
9 WHO model list: revised in December 1995. WHO Drug Information 1995:9(4).
10 J.W. Poole, G. Owen, J. Silverio, J.N. Freyhof, S.B. Rosenman, Curr. Therap. Res. 10 (1968) 292.
11 E. Shefter, H. L. Fung, & O. Mok, (1973). J. Pharm. Sci. 62, 791−794.

12 G. Mandell, M. Sande, (1980); P. Frank, .J. Nayler, H. Smith,(1961); W. Kaufmann, K. Bauer, (1963); D. Johnson, H. Hardcastle, (1964); D. Johnson, S. Wolfe, (1964).
13 P. Doylo, C. Nayler, C. Smith, R. Stove, Nature 191 (1961) 1091–1092
14 M. C. O. Ezeibe, G. N. Anosa, O. K. Okorie, N. P. Elendu- Eleke, O. N. Okoroafor, A. A. Ngene, O. N. Chikelu, Health Vol. 4, No 9 (2012) 675−678.
15 M. O. Boles, R. J. Girven, ActaCryst. (1976)B32, 2279−2284.
16 J. C. Burley, J. V. Streekand, P. W. Stephens, ActaCryst. (2006) E62, o797−o799.
17 V. Crupi, D. Majolino, M.R. Mondello, P. Migliardo, V. Venuti, J. Pharm. Biomed. Anal.29 (2002) 1149.
18 G. Fini, J. Raman Spec. 35 (2004) 335.
19 C. Baraldi, A. Tinti, S. Ottani, M.C. Gamberini, Journal of Pharmaceutical and Biomedical Analysis 100 (2014) 329–340.
20 M.J. Frisch, G.W. Trucks, H.B. Schlegel. G.E. Scuseria, J.R. Cheeseman, M.A. Robb, G. Scalmani, V. Barone, B. Mennucci, G.A. Petersson, H. Nakatsuji, M. Caricato, X. Li, H.P. Hratchian, A.F. Izmzylov, J. Bloino, G. Zheng, J.L. Sonnenberg, M. Hada, M. Ehara, K. Toyota, R. Fukuda, J. Ishida, M. Hasegawa, T. Nakajima, Y. Honda, O. Kitao, H. Nakai, T. Vreven, J.A. Montgomery Jr., J.E. Peralta, F. Ogliaro, M. Bearpark, J.J. Heyd, E. Brothers, K.N. Kudin, V.N. Staroverov, R. Kobayashi, J. Normand, A. Raghavachari, A. Rendell, J.C. Burant, S.S. Iyengar, J. Tomasi, M. Cossi, N. Rega, J.M.Millan, M. Klene, J.E. Knox, J.B. Cross, V. Bakken, C. Adamo, J. Jaramillo, R. Gomperts, R.E. Stratmann, O. Yazyev, A.J. Austin, R. Cammi, C. Pomelli, J.W. Ochterski, R.L. Martin, K. Morokuma, V.G. Zakrzewski, G.A. Voth, P. Salvador, J.J. Dannerberg, S. Dapprich, A.D. Daniels, J. Farkas, B. Foresman, J.V. Ortiz, J. Cioslowski, D.J. Fox, GAUSSIAN 09, Revision, Gaussian, Inc., Wallingford CT, 2009.
21 P. Hohenberg, W. Kohn, Phys. Rev. B 136 (1964) 864–871.
22 W. Kohn, L. Sham, Phys. Rev. A 140 (1965) 1133–1138.
23 C.T. Lee, W.T. Yang, R.G. Parr, Phys. Rev. B 37 (1988) 785–789.
24 A.D. Becke, J. Chem. Phys. 98 (1993) 5648–5652.
25 R.G. Parr, W. Yang, Density Functional Theory of Atoms and Molecules, Oxford University Press, New York, 1989.
26 P.J. Stephens, F.J. Devlin, C.F. Chabalowski, M.J. Frisch, J. Phys. Chem. 98 (1994) 11623.
27 J.M.L. Martin, C. Van Alsenoy, Gar2Ped, University of Antwerp, Antwerp, 1995.
28 P. Pulay, G. Fogarasi, F. Pang, J.E. Boggs, J. Am. Chem. Soc. 101 (1979) 2550– 2560.
29 G. Fogarasi, X. Zhou, P.W. Taylor, P. Pulay, J. Am. Chem. Soc. 114 (1992) 8191–8202.
30 A. Frisch, A.B. Nielson, A.J. Holder, GaussView User Manual, Gaussian Inc, Pittsburgh, P.A., 2005.
31 G.A. Zhurko, D.A. Zhurko, Chemcraft, 2005, http://www.chemcraftprog.com.
32 E.D. Glendening, A.E. Reed, J.E. Carpenter, F. Weinhold, NBO 3.0 Program Manual, Theoretical Chemistry Institute, University of Wisconsin, Madison, WI, 1996.
33 R.F.W. Bader, Atoms in Molecules, A Quantum Theory, Oxford University Press, Oxford, (1990).
34 R.F.W. Bader, S.G. Anderson, A.J. Duke, J. Am. Chem. Soc. 101 (1979) 1389.
35 R.F.W. Bader, T.S. Slee, D. Cremer, E. Kraka, J. Am. Chem. Soc. 105 (1983) 5061.
36 R.F.W. Bader, P.J. MacDougall, J. Am. Chem. Soc. 107 (1985) 6788.
37 R.F.W. Bader, J.R. Cheeseman, In AIMPAC Ed., (2000).
38 S.F. Boys, F. Bernardi, Mol. Phys. 19 (1970) 553–566.
39 R.G. Pearson, J. Org. Chem. 54 (1989) 1430–1432.
40 R.G. Parr, R.G. Pearson, J. Am. Chem. Soc. 105 (1983) 7512–7516.
41 P. Geerlings, F.D. Proft, W. Langenaeker, Chem. Rev. 103 (2003) 1793–1874.
42 R.G. Parr, L. Szentpaly, S. Liu, J. Am. Chem. Soc. 121 (1999) 1922–1924.
43 P.K. Chattaraj, U. Sarkar, D.R. Roy, Chem. Rev. 106 (2006) 2065–2091.
44 J. A. Padro´n, R. Carasco, R. F. Pello´n. J Pharm Pharmaceut Sci. 5 (2002) 258–266.
45 R. P. Verma, C. Hansch. Bioorg Med Chem. 13 (2005) 2355–2372.
46 R. P. Verma, A.Kurup, C.Hansch.Bioorg Med Chem. 13 (2005) 237–255.
47 S. Gunasekaran, R.A. Balaji, S. Kumaresan, G. Anand, S. Srinivasan, Can. J. Anal. Sci. Spectrosc. 53 (2008) 149–161.
48 P.W. Atkins, Physical Chemistry, Oxford University Press, Oxford, 2001.
49 K. Fukui, Science 218 (1982) 747.
50 K. Fukui, T. Yonezawa and H. Shingu, J. Chem. Phys. 20, 722 (1952).
51 D. F. V. Lewis, C. Ioannides, D. V. Parke, Xenobiotica 24 (1994) 401−408.
52 D. C. Ghosh, J. Jana, Current Science, 4 (1999) 76.
53 DOI: 10.1080/08927022.2015.1089996.
54 F. Weinhold, C. R. Landis, Chemistry Education: Research and Practice (2001) 2291.
55 J. P. Foster, F. Weinhold, Journal of the American Chemical Society 102 (1980) 7211.
56 E. D. Glendening, F. Weinhold, Journal of Computational Chemistry 19 (1998) 6593.
57 N. Gonohe, H. Abe, N. Mikami, M. Ito, J. Phys. Chem. 89 (1985) 3642–3648.
58 M. Gutowski, G. Chalasinski, J. Chem. Phys. 98 (1993) 4540–4554.
59 J. Zyss (Ed.), Molecular Nonlinear Optics: Materials, Physics and Devices, Academic Press, Boston (1993).
60 M. Albota, D. Beljonne, J.L. Brédas, J.E. Ehrlich, J.Y. Fu, A. A. Heikal, S. E. Hess, T. Kogej, M. D. Levin, S. R. Marder, D. McCordmaughon, J. W. Perry, H. Rockel, M. Rumi, C. Subramaniam, W. W. Webb, I. L. Wu and C. Xu, Science, 281 (1998) 1653.
61 A. M. McDonagh, M. G. Humphrey, M. Samoc and B. Luther-Davies, Organometallics, 18 (1999) 5195.
62 C. E. Powell, J. P. Morrall, S. A. Ward, M. P. Cifuentes, E. G. A. Notaras, M. Samoc and M. G. Humphrey, J. Am. Chem. Soc., 26 (2004) 12234.
63 A. J. Garza, O. I. Osman, N. A. Wazzan, S. Khan, A. M. Asiri, G. E. Scuseria, Theor.Chem. Acc. 133 (2014) 1458.
64 U. Koch, P. Popelier, J. Phys. Chem. A 99 (1995) 9747–9754.
65 I. Rozas, I. Alkorta, J. Elguero, J. Am. Chem. Soc. 122 (2000) 11154–11161.
66 E. Espinosa, E. Molins, C. Lecomte, Chem.Phy. Letters 285 (1998) 170−173.
67 G.A. Guirgis, P. Klaboe, S. Shen, D.L. Powell, A. Gruodis, V. Aleksa, C.J. Nielsen, J. Tao, C. Zheng, R.J. Durig, J. Raman Spectrosc. 34 (2003) 322.
68 P.L. Polavarapu, J. Phys. Chem. 94 (1990) 8106.
69 H. Yoshida, K. Takeda, J. Okamura, A. Ehara, H. Matsurra, J. Phys. Chem. A 106 (2002) 3580–3586.
70 R.M. Silverstein, G.C. Bassler, Spectrometric Identification of Organic Compounds, second ed., JohnWiley and Sons Inc., New York, 1967.
71 J. Coates, Interpretation of Infrared Spectra, A Practical Approach, John Wiley & Sons Ltd, Chichester, 2000.

Table of contents

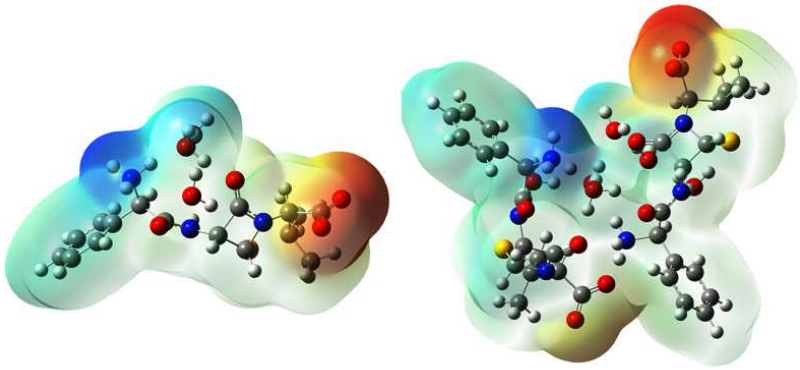

Optimized structure and active sites of ampicillin trihydrate calculated using monomeric and dimeric model